Two-photon excited room-temperature luminescence of CdS in the femtosecond regime

J.-F. Lami and C. Hirlimann
Groupe d'Optique Non-Linéaire et d'Optoélectronique, Institut de Physique et Chimie des Matériaux de Strasbourg, Unité Mixte CNRS-ULP (UMR 7504), 23 rue du Lœss, Boîte Postale 20 CR, F-67037 Strasbourg Cedex, France
(Received 15 March 1999)

We present a dynamic study of the room-temperature, two-photon excited luminescence in CdS. When exciting the medium with red (2 eV), 100-fs-lasting pulses of intensity 9.4 GW/cm^2, a strong two-photon absorption, with coefficient $\alpha_2 = 2.7$ cm/GW, creates 1.6×10^{16} cm^{-3} highly out-of-equilibrium carrier pairs. The overall kinetic energy relaxation time of these carriers has been measured to be of 350 fs and their final states have been determined as being shallow residual localized states in the band gap. From these states, potential energy relaxation gives rise to a stimulated emission of green (2.45 eV) light. The dynamics of this emission has been studied using a time resolved gain measurement experiment, which indicates a 200-fs duration for the highest excitation intensities (20 GW/cm^2). [S0163-1829(99)10631-3]

I. INTRODUCTION

A strong green light emission takes place at room temperature in cadmium sulfide when shining a crystal with short 100-fs-lasting light pulses in the visible or near-infrared parts of its transparency wavelength range. This spectacular anti-Stokes emission is a direct consequence of a strong two-photon absorption taking place in the semiconductor. It is the aim of this work to explore the various mechanisms underlying this effect.

In these experiments we used as a sample bulk cadmium sulfide in the form of high quality platelets, 50 and 130 μm thick, vapor grown in an argon atmosphere, in a thermal gradient furnace. During the growth process,[1] the argon flux was kept between 0.3 and 3 l/min and the furnace maximum temperature between 1050 and 1090 °C. X-ray scattering measurements showed that the sample structure is hexagonal wurtzite. The optical *c* axis lies in the plane of the platelet; its direction was determined through linear optical transmission measurement at the band gap energies.[2] Optical, room-temperature transmission measurement showed that the gap of the sample was 2.48 eV, when the electric field of the light pulses is parallel to the *c* axis. From low temperature excitonic luminescence bandwidth and intensity measurements the residual impurity content was estimated to be less than 10^{15} cm^{-3}.

Optical pulses, 100 fs in duration, at 627-nm central wavelength (2 eV), were generated using a dispersion compensated colliding pulse mode-locked (CPM) laser oscillator.[3] These pulses were amplified[4] using a doubled Nd:YAG laser (YAG denotes yttrium aluminum garnet) as a pump, at a 20-Hz repetition rate, up to an energy of 1.5 μJ, allowing us to reach focused intensities up to 150 GW/cm^2. In transmission pump-probe experiments the pump beam was focused down to an e^{-2} radius of 36 μm. The probe pulses were kept down to intensities less than a few percent of the pump intensity and the pump was linearly cross polarized with the probe. The pump polarization was set to be parallel to the *c* axis of the bulk CdS crystal in order not to induce any spurious birefringence. Scattered light from the pump was rejected by linearly analyzing the light coming out of the sample parallel to the probe polarization. The duration of the light pulses was determined by replacing the sample with a 200-μm-thick, phase matched, KH_2PO_4 (KDP) crystal and recording an intensity envelope autocorrelation trace. At the exit of the amplifier a prism-pair optical compressor was adjusted in order to compensate for the positive group velocity dispersion induced by the various optical elements placed on the light path, so that the optical pulses (with a sech^2 envelope) were quasi Fourier transform limited with $\Delta\nu\Delta t$, spectral width times duration relationship equal to 0.34. When necessary, a broadband white light continuum was generated by tightly focusing 0.7-μJ pulses onto a 200-μm-thick ethylen glycol jet.[5,6]

The light transmitted through the sample is spectrally analyzed using a 25-cm focal length spectrograph. A photodiode array mounted at the spectrograph exit port detects the diffracted light. An optical multichannel analyzer (OMA III) drives the photodiode array and digitizes the signal, enabling data processing.

II. LINEAR ABSORPTION AND EMISSION

Figure 1 shows measurements of the light transmission through a 50-μm-thick CdS sample. In a simple model where a semiconductor is made of parabolic valence and conduction bands, vertical optical transitions of an electron from the valence to the conduction band are at the origin of the absorption of photons with energy $\hbar\omega$: $\alpha(\omega) \propto (1/\hbar\omega)\sqrt{\hbar\omega - E_g}$ where E_g is the energy gap. This expression is only valid for photon energies larger than the gap energy and the law describes the photocreation of delocalized carriers. Once a measurement of the absorbance αd is made one can plot the quantity $(\alpha d)^2 E^2$ as a function of the energy E as shown in Fig. 1(a). The linear part of the plot directly gives a quantitative value of the energy of delocalized electrons in the material. In our sample the minimum energy for these delocalized electrons is 2.479 eV when the polarization of the incident light is parallel to the *c* axis of the crystal, a value which is in good agreement with excitonic gap measurements.[7,8]

Below the band gap of a semiconductor, residual absorp-

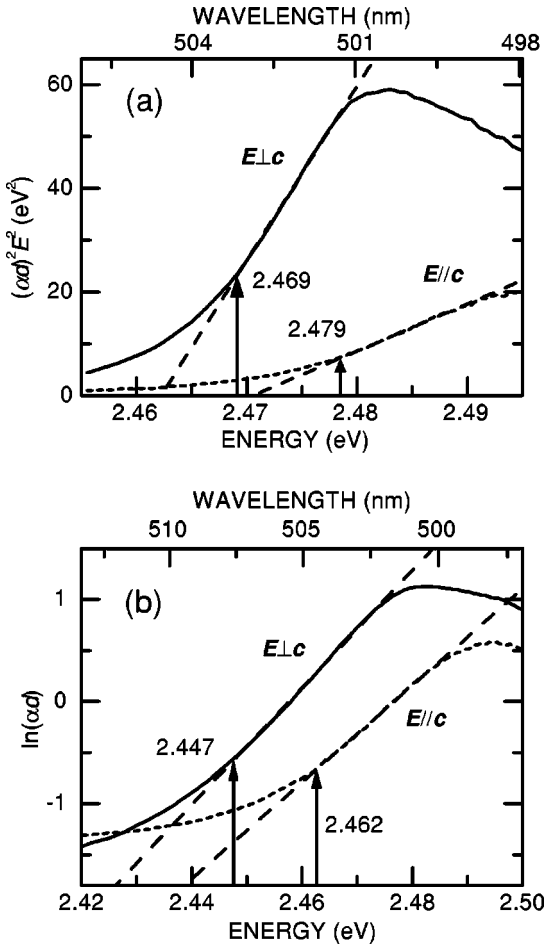

FIG. 1. Plots of the modified absorbance of a 50-μm-thick CdS sample for incoming light polarization parallel or perpendicular to the optical axis c of the crystal. (a) Plot of the squared energy-absorbance product, versus incoming photon energy, showing, in the linear part, the extended state energy range of the crystal. (b) Plot of the natural logarithm of the absorbance versus incoming photon energy: the linear part indicates the energy range of the shallow localized states in the crystal. The high energy saturation and decrease of the curves is an artifact related to the weakness of the transmitted signal.

tion does take place due to impurities and defect localized states. It has long been recognized that this absorption varies mostly as an exponential function of the incident photon energy as can be seen in the empirical Urbach law:[9,10] $\alpha(\omega,T)=\alpha_0\exp[-\sigma(E_0-\hbar\omega)/k_BT]$, where α_0, E_0, and σ are constant parameters for a given temperature T, and k_B stands for Boltzmann's constant. From this expression it is clear that the energy range of localized states in the material is given by the linear part of a plot of the natural logarithm of the absorbance versus photon energy. This plot is shown in Fig. 1(b). The minimum energy of the localized states in our specific sample is then 2.462 eV when the polarization of the incident light is parallel to the optical axis and 2.447 eV for the orthogonal polarization.

As can be seen in Fig. 2, the two-photon excited luminescence spectral band is coincident with the localized states of lowest energy in the crystal. Emission peaks at 2.45 eV (507 nm) and the spectrum is 18 meV (3.7 nm) wide at half maximum. As the sample naturally has highly parallel faces with

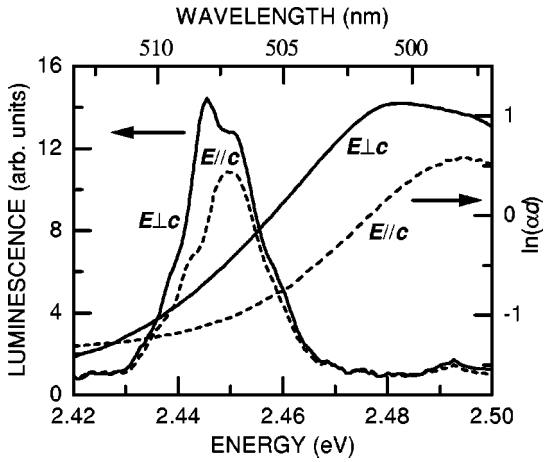

FIG. 2. Right vertical scale: plot of the natural logarithm of the absorbance of a 50-μm-thick CdS sample for light polarization parallel and perpendicular to the c axis of the crystal. Left vertical scale: plot of the room-temperature two-photon excited green luminescence spectrum of CdS under femtosecond excitation with pulses lasting 100 fs and having an intensity of 22 GW/cm^2.

a high 20% reflectivity Fabry-Pérot interferences occur in the sample, resulting in the dual peak modulation observed on the emission spectrum. As the index of refraction changes from one polarization of the light to the other, the relative phase of the interference pattern in the emission spectrum does shift when going from one polarization to the other. The one electron band structure of cadmium sulfide is still under theoretical discussion[11] but it is known that the extrema of the valence and conduction band are in the center of the Brillouin zone, cadmium sulfide is a direct semiconductor.[12] At the center of the Brillouin zone ($k=0$) the degeneracy of the valence band is split both by the crystal field and by the spin-orbit coupling leading to three vertical optical transitions between three valence bands and the conduction band.[13,14] Because of the band structure, specific selection rules for optical transitions do apply. Therefore optical transitions between the highest valence band (band A with band gap energy of 2.48 eV) and the conduction band are forbidden for light polarization parallel to the c axis, while they are allowed between both deepest valence bands (band B and band C with band gap energies, respectively, of 2.495 eV and 2.557 eV) and the conduction band for light polarization parallel and perpendicular to the c axis. As a first consequence the luminescence intensity is weaker when the polarization of the exciting light is parallel to the c axis of the crystal because of a weaker absorption in this geometry (see Fig. 2). Furthermore, in a separate experiment, we checked that the polarization of the emitted light is always orthogonal to the c axis direction independent of the polarization direction of the incoming light. This behavior is typical of the highest valence band (A), so that this result clearly indicates that only carriers thermalized to the bottom of their band are involved in the radiative recombination process. These observations evidence that the luminescence is emitted from shallow localized states inside the band gap associated to the valence band A.

III. TWO-PHOTON ABSORPTION

Since its observation by Kaiser and Garret,[15] two-photon absorption (TPA) has been widely studied under various ex-

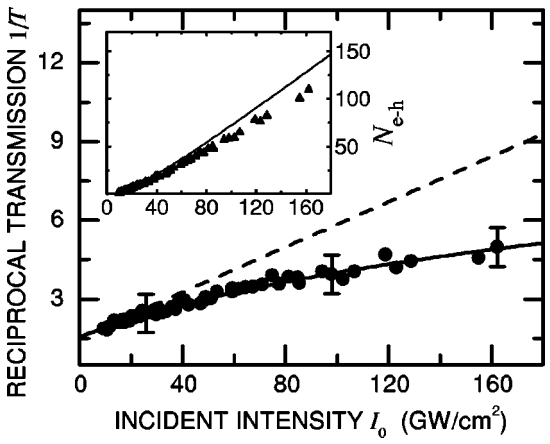

FIG. 3. The solid circles are a plot of the measured reciprocal transmission versus incident intensity. Solid line: theoretical variation for a hyperbolic intensity dependence of the two-photon absorption coefficient. Dashed line: theoretical variation for a constant two-photon absorption coefficient. In the inset is shown the density $N_{e\text{-}h}$ (in 10^{16} cm^{-3} units) of photocreated electron-hole pairs versus the incident intensity I_0 (in GW/cm^2). Solid triangles: $N_{e\text{-}h}$ calculated from the experimental data. Solid line: theoretical $N_{e\text{-}h}$ for a constant two-photon absorption coefficient.

perimental conditions and in various semiconductors. In cadmium sulfide, the two-photon absorption coefficient α_2 was measured in 1969. In the literature, its measured value ranges from 3.2 to 70 cm/GW (see Ref. 16 for a review). A theoretical value of 4.87 cm/GW has been computed by van Stryland, Woodall, Vanherzeele, and Soileau.[17] Despite the wide dispersion in the measured values of the TPA coefficient, all the most recent values tend toward the theoretical value. This can be explained by the appearance of femtosecond lasers which allow avoidance of absorption variations due to carrier effects which typically have a characteristic time of hundreds of femtoseconds.

Under our experimental conditions, a 130-μm-thick crystal is shone on by 100-fs, 2-eV optical pulses with intensities ranging up to 160 GW/cm^2. For carrier densities of the order of 10^{18} cm^{-3}, band gap renormalization in CdS is overestimated to be 45 meV.[18] The fundamental 2 eV photon energy misses the equilibrium band gap energy by 480 meV, and therefore one-photon absorption can be neglected. The transmitted intensity I_t' is recorded as a function of the incident intensity I_0. Figure 3 shows the superposition of a set of records where the reciprocal transmission $(1/T = I_0/I_t')$ is plotted as a function of the incident intensity. In a simple model, the variation of the transmitted intensity as a function of the incident intensity is given by the integration over the thickness of the sample of the following differential equation when one-photon absorption and orders higher than two are neglected:

$$dI = -\alpha_2(I) I^2 dz. \tag{1}$$

The unsaturated solution of Eq. (1) with $\alpha_2(I) = \alpha_2^0$, the low intensity response of the material, corresponds to the dashed line in Fig. 3. At intensities higher than 30 GW/cm^2, the experimental data strongly depart from this unsaturated model. This anomalous behavior cannot be explained by one-photon absorption by the photocreated carriers, nor by three-photon or higher-order absorption which both would yield an opposite effect, i.e., a decrease in the transmission. In preliminary experiments, we checked that the surface crystal experiences only shallow degradation of the order of 1 μm in depth, when the most intense light beam is focused onto the entrance surface. The surface roughness does not scatter the light in a way that affects the transmission measurements since the intensity of the outcoming beam does not change when decreasing the intensity after having reached the maximum intensity. During the two-photon absorption process, which lasts as long as the pulse duration, the nonlinear change of the refractive index for an excitation pulse of 10 GW/cm^2 is $\Delta n = -0.005$ and the corresponding relative variation of the reflection coefficient is negligible, $\Delta R/R = -0.004$.[19] At 150 GW/cm^2 the maximum expectable index variation is $\Delta n = -0.075$ and $\Delta R/R = -0.06$. This is still small enough to be negligible, at least within our experimental uncertainty. A relative increase of the transmission due to a decrease of the reflections in the sample cannot account for our observation. The refractive index variations are negative because the photon energy corresponds to more than 70% of the band gap energy.[20]

The beam inside the crystal experiences defocusing because of the negative variations of the refractive index. This effect yields a spatial expansion of the beam and consequently a decrease in the intensity. However, according to Ref. 21, where a theoretical model based on the nonlinear wave equations is developed, the defocusing effect is negligible under our experimental conditions. The spatial expansion of the outcoming beam at the exit surface of the crystal is less than 0.05% of the incident beam extension at the entrance surface. Furthermore, the negative nonlinear refractive index and the positive group velocity inside the crystal generate at the higher intensities a self-compression[22] of the optical pulses of about 20%. This pulse compression induces an increase of the beam intensity inside the crystal which overrules the effects of the defocusing.

The experimental data can only be understood as an interband two-photon absorption saturation.[23] This dynamic saturation is possible only because the pulse duration is shorter than the thermalization time of the photocreated carriers (as shown in Sec. IV) and of course because of the high intensities reached. In the inset in Fig. 3 the density of photocreated carrier pairs, calculated from the number of absorbed photons, is plotted as a function of the incident intensity. It varies from 1.6×10^{16} cm^{-3} when $I_0 = 9.4$ GW/cm^2 (1.7×10^{10} absorbed photons) to 10^{18} cm^{-3} when $I_0 = 162$ GW/cm^2 (10^{12} absorbed photons). Again the experimental variation departs from the expected variation when no saturation is taken into account (solid line in the inset in Fig. 3). It is noticeable that no saturation plateau is observed due to the competition between state filling and thermalization of the carriers. In order to model the saturation, we used a hyperbolic approximation:[24]

$$\alpha_2(I) = \frac{\alpha_2^0}{1 + I/I_{\text{sat}}}, \tag{2}$$

where α_2^0 is the low intensity response of the material and I_{sat} the saturation value of the intensity for which α_2^0 is divided by 2. To take into account the light reflection R at the en-

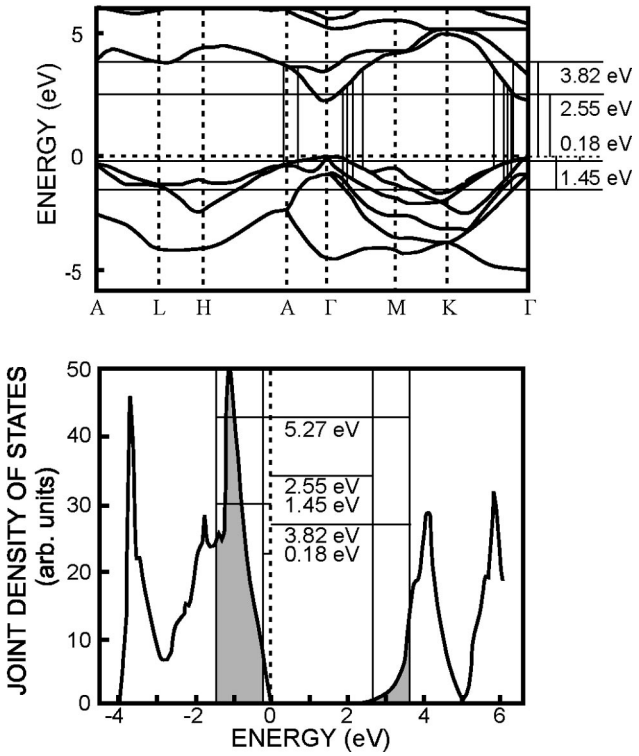

FIG. 4. Computed band structure and joint density of states for hexagonal CdS from Ref. 26. The vertical solid lines in the band structure graph correspond to the possible 4-eV optical transitions. The gray regions indicate the densities of electronic states which might be involved in the 4-eV transitions.

trance and exit faces of the sample the incident intensity I_0, respectively, the transmitted intensity without reflection I_t, is replaced by $I_i = I_0(1-R)$, respectively, by $I_t' = I_t(1-R)$. For a thickness d of the sample the formal solution of Eq. (1) then reads as

$$\frac{1}{I_0(1-R)} - \frac{1-R}{I_t'} + \frac{1}{I_{\mathrm{sat}}} \ln \left| \frac{I_t'}{I_0(1-R)^2} \right| = -\alpha_2^0 d. \qquad (3)$$

From this expression the reciprocal transmission ($1/T = I_0/I_t'$) has been numerically evaluated and used to fit the experimental data, as shown as a solid line in Fig. 3. From this fit one finds $\alpha_2^0 = \alpha_2(I \ll I_{\mathrm{sat}}) = 2.7$ cm/GW, $R = 19\%$, values which are in close agreement with the ones found in the literature.[17,25] The good agreement obtained for the linear reflectivity further confirms the harmlessness of the degradation of the sample surface already mentioned. From Eq. (3) we deduce a saturation intensity for the two-photon absorption process $I_{\mathrm{sat}} = 65$ GW/cm^2.

Although band structure calculations for semiconductors are not totally reliable for interpreting experimental results, we considered the calculation performed in Ref. 26 which gives, for hexagonal CdS, both the band structure and the associated electronic state density. Examination of the possible electronic transitions, under 4-eV two-photon excitation, which may happen in the band structure (see Fig. 4), allows us to determine which electronic states participate in the process. The participating holes lie in a 1.27-eV-wide band around -815 meV, when the energy is measured from the top of the valence band, while the contributing electrons are distributed in a 1.27-eV-wide band lying 50 meV above the minimum of the conduction band. (No 4-eV vertical transition is possible in the center of the Brillouin zone.) More precisely, the 4-eV optical transitions can occur from valence states lying between -1.45 and -0.18 eV, to conduction states lying between 2.55 and 3.82 eV. The hole band is coincident with a peak in the valence state density while the electron band lies in the slowly increasing conduction state density (see the joint density of states graph in Fig. 4). The density of states available for the holes is roughly 30 times larger than the one available for the electrons, therefore the saturation of the two-photon absorption saturation is due to the electrons.

IV. PHOTOCREATED CARRIER DYNAMICS

As shown in the preceding section, the two-photon absorption yields a strongly out-of-equilibrium population of carriers. At the time of their photocreation, the electrons, respectively, the holes, have a kinetic energy excess of $(2\hbar\omega - E_g)\mu_r/m^* = 1.2$ eV, respectively, 0.3 eV, where E_g is the band gap energy, μ_r the reduced mass, and m^* the effective mass of the electron, respectively, of the hole. The carrier pairs do lose their kinetic energy excess mostly by interacting with longitudinal optical (LO) phonons. The thermalized carriers have a Fermi-Dirac distribution of their energies. Using an analytical approximated formula[27] of the Fermi-Dirac integrals with $\pm 0.5\%$ error, it is possible to compute the temperatures and the chemical potentials of the thermalized electrons (T_e, μ_e) and holes (T_h, μ_h). For an initial density of photocreated carriers of 10^{18} cm^{-3}, $T_e = 13\,900$ K, $T_h = 3500$ K, $\mu_e = -5.5$ eV, and $\mu_h = -2$ eV (the top of the valence band corresponding to the zero energy).

Because the nonlinear index of refraction inside the CdS crystal is negative the beam experiences defocusing. During the optical excitation, the value of the nonlinear refractive index is mostly governed by two-photon absorption and optical Stark effect, and in a much less significant way by linear Stark effect and Raman scattering.[20] We actually measured this instantaneous nonlinear refractive index in a separate experiment:[22] $n_2 = -3 \times 10^{-13}$ cm/W. After the optical excitation the nonlinear refractive index is only determined by carrier effects like band filling,[28–31] free-carrier absorption,[32,17] band gap renormalization,[30,33,34] screening of the Coulomb interaction in a plasma,[28,30,33] and crystal heating.[35,36] Under our experimental conditions, band filling is the main contributor to the variations of the refractive index. Only band filling, yielding a blueshift of the optical gap, has been observed in materials similar to CdS under two-photon excitation.[37] Band gap renormalization due to ''hot'' nonthermal carrier populations has not yet been observed. The cross section[32,38] of the free-carrier absorption is equal to about 10^{-18} cm^2 and therefore can be neglected for 100-fs-lasting pulses.[39] The screening of the Coulomb interaction is also negligible because of the room-temperature operation. No crystal heating is observed under our experimental conditions due to the low repetition rate of 20 Hz of the laser amplifier and the low 1-μJ energy of the pulses. The crystal has enough time to cool down during the 50 ms

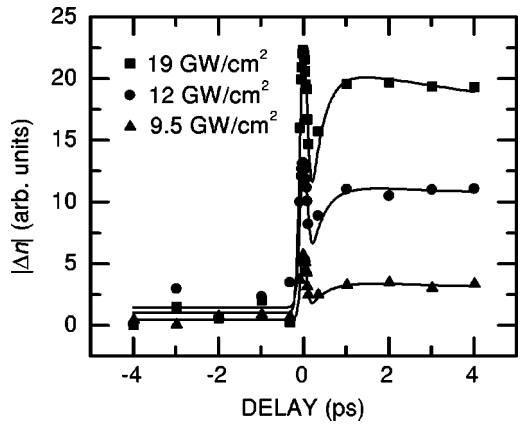

FIG. 5. Absolute variations $|\Delta n|$ of the refractive index versus time delay between pump and probe for three pump intensities. These curves are obtained by measuring the integrated intensity of the probe spectrum through an aperture situated in a beam region where defocusing is important: the light intensity decreases with a negative index variation. The background signal is subtracted and the absolute value of the signal is taken. Solid lines correspond to fits calculated with the three-level model described in the text.

separating two consecutive pulses of about 1-μJ energy to avoid any cumulative effects.

We performed a degenerate pump-probe experiment in order to investigate the dynamics of the relaxation processes. Recording of the index dynamics can be done by simply transforming the induced defocusing into an intensity variation by means of an aperture placed in front of the detector.[40] To a maximum transmitted light intensity corresponds a minimum index variation and vice versa. The mean value of the transmitted intensity was automatically calculated over five recordings for each value of the time delay between the pump and the probe in order to improve the signal to noise ratio.

Figure 5 shows the variation of the probe integrated intensity versus time delay, for three pump intensities following the procedure outlined above. At zero time delay, an instantaneous index change can be observed. This has been shown in a separate experiment to be due to cross-phase modulation corresponding to a dynamic electric field induced Kerr effect.[22] The shape of the early time response is simply the autocorrelation function of the light pulses. Its width is in good agreement with that of the separately measured KDP autocorrelation functions. At this time two-photon absorption creates carrier populations with a large excess of kinetic energy, an absorption change is created 1.5 eV above the equilibrium band gap energy. The Kramers-Kronig relations are energetically resonant with the absorption change and therefore negligible change at 4 eV of the index of refraction and intraband electronic population can be expected at 2 eV arising from the carrier population. At longer time delays the carrier population thermalizes at the bottom of the conduction and valence bands having now an excess energy which is only 480 meV against the 2-eV photon energy. The thermalized carrier population induces an index change which can be seen in Fig. 5 as a signal rise following the instantaneous response. After this thermalization process has taken place, the carriers relax their potential energy and this shows up in Fig. 5 as a slow decay along the last 3 ps.

The index variation results have been modeled using a set of coupled dynamic differential equations describing the evolution of the electronic populations in a three-level system:

$$\frac{dN(t)}{dt} = \frac{n(t)}{\tau_{\text{th}}} - \frac{N(t)}{\tau_r}, \tag{4a}$$

$$\frac{dn(t)}{dt} = \Gamma^2\left(\frac{t}{t_0}\right) - \frac{n(t)}{\tau_{\text{th}}}. \tag{4b}$$

In this set of equations $N(t)$ is the thermalized population of carriers, proportional to the long lasting index change, $n(t)$ is the population of out-of-equilibrium photocreated carriers, τ_{th} is the intraband thermalization time, and τ_r is the electron-hole interband recombination time. Finally, $\Gamma(t/t_0)$ is the pulse intensity envelope of duration t_0 which, in this simple model, has been chosen as a squared hyperbolic secant function. From this set of equations an analytical solution for $N(t)$ is derived which is proportional to the index change. To account for the instantaneous response, which is not included in Eq. (4), the intensity autocorrelation function $\Gamma'(t/t_0)$ of the pulse is added as $aN(t)+b\Gamma'(t/t_0)+c$ (the parameter c accounts for small offsets in the experimental data). A least squares fit to the experimental data following the Cholesky method[41] is then performed. The results of this calculation are shown in Fig. 5 as solid lines. From this model we deduce a thermalization time $\tau_{\text{th}}=350$ fs, independent of the excitation intensity, and a radiative relaxation time $\tau_r=100$ ps for the lower excitation intensities which decreases to 40 ps for the highest intensity (19 GW/cm^2).

The transfer of the carrier kinetic energy to the lattice of the crystal is efficiently done via their interactions with the polar LO phonons, the energy of which is 38 meV.[42] In order to thermalize to the bottom of the conduction band, the electrons have to lose a maximum kinetic energy excess of 1.34 eV (see Fig. 4). It means that the ''hottest'' electrons have to interact with 35 LO phonons in order to dissipate their energy excess. From our thermalization time measurement we deduce that the electron-phonon interaction duration should be about 10 fs. This value is about five times shorter than in GaAs,[43,44] due to the more polar character of CdS when compared to GaAs.

V. STIMULATED EMISSION

Under 100-fs photoexcitation strong two-photon absorption takes place which generates carrier pairs with a density as high as 1.6×10^{16} cm^{-3} and a maximum excess kinetic energy of 1.5 eV. These highly out-of-equilibrium carriers thermalize in about 350 fs (see Sec. IV) to the shallow residual localized states described in Sec. II. Once thermalized the carriers create a large electronic population from which stimulated emission can take place. This stimulated emission is evidenced by the duration of the emission process which is less than the 5-ps time resolution of the streak camera (ARP model GMCD1) we used in a preliminary measurement. For ''low'' intensity excitation ($I_0\simeq9$ GW/cm^2) the measured luminescence duration is of the order of 100 ps (see Sec. IV) closer to the values ranging from 0.6 to 1 ns reported in the literature for the spontaneous emission time in CdS at room

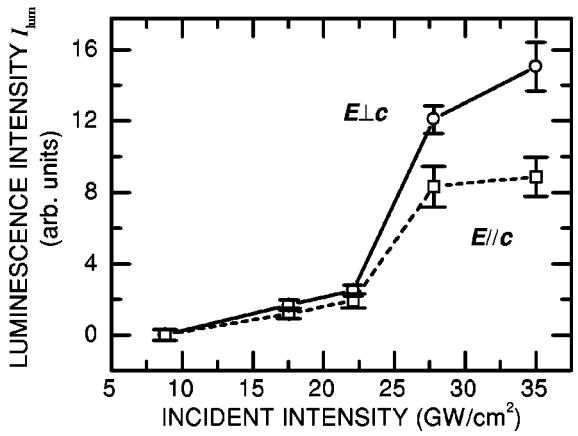

FIG. 6. Stimulated emission threshold for incident light polarization perpendicular (open circles) and parallel (open squares) to the c axis. The threshold intensity I_{th} equals 22 GW/cm^2.

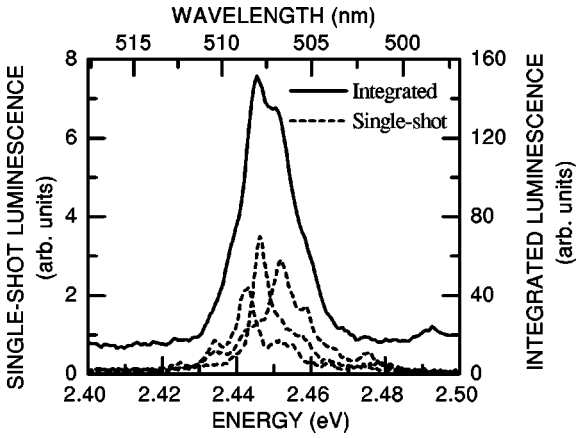

FIG. 7. Luminescence spectra: integrated over several excitation pulses (solid line) and single-shot excitation (dashed lines). In both cases, the incident light polarization is perpendicular to the c axis.

temperature.[45] A sharp drop from 100 to 40 ps is observed in the luminescence duration when the intensity is increased above 20 GW/cm^2.

When measuring the luminescence integrated intensity as a function of the incident light intensity (see Fig. 6), a threshold intensity I_{th} clearly appears around 22 GW/cm^2 for both light polarizations. This threshold behavior is also typical of stimulated emission. The value of I_{th} is in good agreement with the measured intensity for which the recombination time begins to decrease, as described above. Stimulated emission was observed in CdS at room temperature in the 1970s.[46] However, the threshold intensity was found to be more than three orders of magnitude lower than in our case. Such a huge difference can be explained by the differences in the experimental conditions and in the sample quality. In Ref. 46, the light pulses (20 ns in duration, with a photon energy of 1.78 eV) were generated by a ruby laser which is well known to have intensity hot spots in its beam profile. This yields spatial power peaks in the pulse and can lead to an underestimation of the value of the intensity threshold. Furthermore, the nanosecond pulses used deliver much more energy ($\simeq$450 mJ) than the femtosecond pulses generated by the amplified CPM ($\simeq$1.5 μJ). This fact is strongly supported by the comparison of the damage threshold values measured in both cases: 100 MW/cm^2 in Ref. 46, more than 150 GW/cm^2 in our case. Moreover, the CdS crystal used in Ref. 46 is from much lower quality than are ours where no photocurrent can be measured, indicating a very low density of impurities. Finally our value of I_{th} is in good agreement with the most recently published values.[37] In Fig. 6 the luminescence intensity reaches a saturation at higher incident intensities. This saturation behavior is mainly due to the strong defocusing process experienced by the luminescence in the crystal which may lead to an imperfect collection of the luminescence emission. Furthermore, a strong reabsorption of the luminescence emission occurs in the crystal because its energy is obviously resonant with optical transition energies, yielding a decrease of the transmitted luminescence intensity.

Figure 7 shows the luminescence spectra, when integrated over a large number of excitation pulses (solid line), and for single-shot excitation (dashed lines). The single-shot excitations were performed by decreasing both the repetition rate of the Nd:YAG laser pumping the amplifiers to 5 Hz and the accumulation time of the photodiode array in the optical multichannel analyzer to 15 ms. It can be seen that the central position of the single-shot spectra varies from one pulse to the other. However, each single-shot spectrum lies under the integrated spectrum. The fluctuation of the central position of the single-shot spectra is well explained by considering a stimulated emission starting randomly on a noise. Again the Fabry-Pérot fringes mentioned in Sec. II are visible on the single-shot spectra.

As a summary, a density of 1.6×10^{16} cm^{-3} highly out-of-equilibrium carriers is generated by two-photon absorption in a CdS crystal. These photocreated carriers thermalize in 350 fs to shallow residual localized states in the semiconductor band gap. This yields to a population inversion which initiates a stimulated emission starting randomly on a noise. At the highest excitation intensities ($>$20 GW/cm^2), the stimulated emission lasts less than 5 ps.

VI. GAIN DYNAMICS

A nondegenerate pump-probe experiment was performed in order to investigate the gain dynamics of the luminescence in this experiment. The pulses (1.5-μJ, 100-fs, 2-eV photon energy) generated by the amplified CPM are split into equally powerful pump and ''probe'' beams. The ''probe'' beam is tightly focused down onto a 200-μm-thick ethylen glycol jet. A wide-band green filter selects, in the light continuum generated in the jet, pulses with a spectrum centered around 2.45 eV. By crossing the jet and the focusing lenses, the pulse duration is increased because of positive group velocity dispersion. However, a negative group velocity dispersion is generated in a prism-pair compressor positioned after the amplifiers, in order to precompensate for the positive group velocity generated in the next-on-the-light-path optics. This way, the probe-pulse duration is maintained down to 100 fs. Because the prism compressor is positioned before the splitting of the pump and ''probe'' beams, the group velocity dispersion is overcompensated in the pump pulse, the duration of which is slightly increased. This guarantees that the probe-pulse duration is at least not longer than the pump-pulse duration. In any case these duration extensions

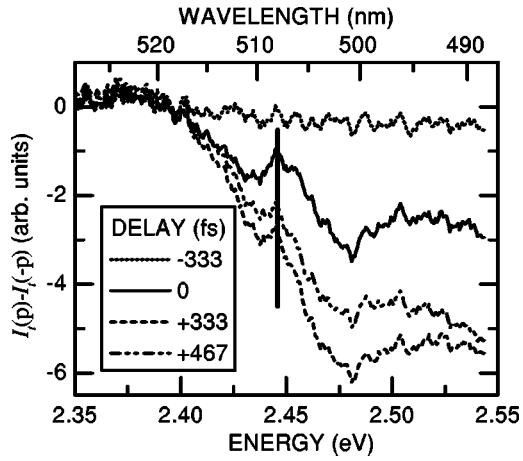

FIG. 8. Differential spectra of the transmitted intensity of the probe pulse for three different delays between pump and probe: dotted line, −333 fs; solid line, temporal coincidence; dashed line, +333 fs; and dashed-dotted line, +467 fs. The vertical line indicates the luminescence energy position (see Fig. 7) and the position of the gain peak. The pump intensity is 30 GW/cm^2.

remain negligible.[6] Eventually the pump and probe pulses are focused down to an e^{-2} radius of 60 μm on the CdS crystal by means of a focusing lens with an f number equal to 1.5. The pump and the probe beams are spatially overlapped inside the crystal. Because the luminescence emission is kept polarized perpendicular to the c axis, the probe-pulse polarization is rotated to be also perpendicular to the c axis, while the pump-pulse polarization remains parallel to the c axis. An analyzer placed before the spectrograph rejects all scattered light from the pump. A delay line mounted on a motorized translation stage allows us to vary the delay between the pump and the probe pulses. The temporal overlap is determined by a nondegenerate defocusing experiment similar to the one described in Sec. IV and Ref. 22.

Figure 8 shows differential spectra of the transmitted probe pulse for three different delays between the pump and the probe pulses. The differential spectra are recorded by subtracting the spectrum of the transmitted-probe pulse in the absence of the pump pulse $I_t(-p)$ from the spectrum of the transmitted-probe pulse in the presence of the pump pulse $I_t(p)$. When the pump pulse hits the sample after the probe pulse, the differential spectrum is flat around zero (dotted line in Fig. 8). When the delay becomes positive a valley appears at high energy (see Fig. 8). This is due to the strong defocusing experienced by the probe beam that leads to an imperfect collection of the light and consequently a decrease in the transmitted-probe intensity. At the luminescence energy position (vertical line in Fig. 8) a peak appears corresponding to the emission stimulated by the probe pulse. The gain of the stimulated emission can be measured by integrating the peak and subtracting the induced defocusing with a linear fit of the slope under the peak. Figure 9 shows the gain variations as a function of the delay between the pump and the probe pulses for a pump intensity of 22 GW/cm^2, right at the threshold intensity for stimulated emission. The gain dynamics is clearly unsaturated and is a good picture of the temporal profile of the luminescence emission pulses. The gain lasts for about 200 fs. Under these conditions, the optical pumping time is completely determined by

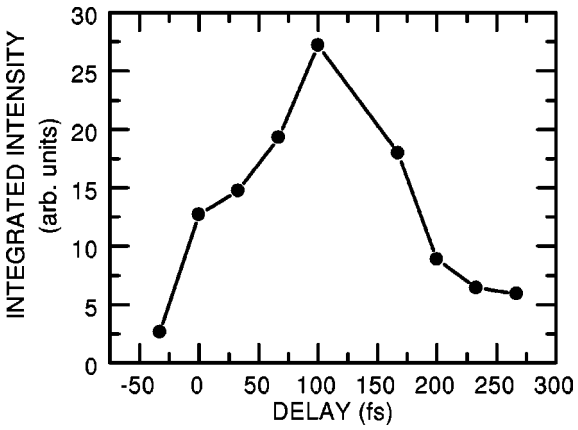

FIG. 9. Gain dynamics with a pump intensity of 22 GW/cm^2, right at the threshold intensity I_{th} for stimulated emission. The gain is unsaturated and lasts for 200 fs.

the thermalization time. The carriers photocreated by the pump pulse have to thermalize to yield the population inversion. The stimulated emission can start spontaneously or on a probe-pulse photon. These two competitive starting processes add extra difficulties to the reproducibility of the experiment.

At higher excitation intensity, the gain dynamics is completely different. Figure 10 shows the gain dynamics for a pump intensity of 30 GW/cm^2, higher than the stimulated emission threshold. The gain presents several oscillations each of which lasts for about 200 fs. This noisy oscillating behavior is the result of the competitive interplay of three noisy processes: optical pumping of a population inversion, stimulated emission, and gain saturation, the net result of which is a rise time and a fall time of the order of 100 fs each. Maxima in the transmitted-probe intensity indicate maximum available gain while dips correspond to gain depletion where the probe experiences no intensity changes. This behavior is similar to the oscillatory emission of the amplified spontaneous emission (ASE) in a multipass amplifier.[47] A model has been developed in Ref. 47 whose predictions are in good agreement with our experimental results (see Fig. 8 in Ref. 47). In both the threshold and high

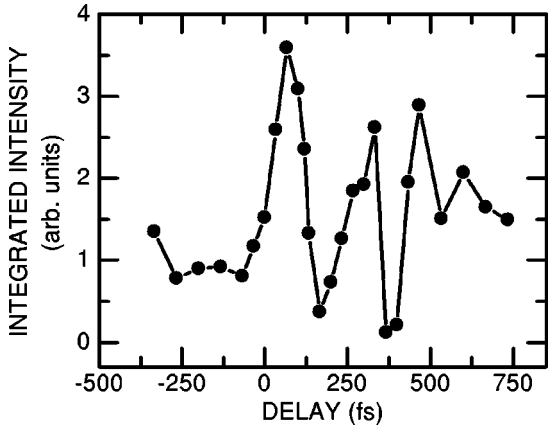

FIG. 10. Gain dynamics with a pump intensity of 30 GW/cm^2 above the threshold intensity I_{th} for stimulated emission. The gain presents several oscillations with a period of about 200 fs.

intensity cases, the 200-fs duration of luminescence pulses is highly compatible with the 5-nm bandwidth of the gain.

VII. CONCLUSION

Using dynamic gain measurement techniques in the femtosecond regime, we have demonstrated the possibility of generating ultrashort 508-nm green light pulses in high quality CdS platelets at room temperature using two-photon absorption excitation. The dynamics of the observed stimulated emission has been shown to be governed by fast carrier thermalization and fast gain saturation.

ACKNOWLEDGMENT

The authors are grateful to M. Joucla for the CdS crystal preparation.

[1] J.-I. Chikawa and T. Nakayama, J. Appl. Phys. **35**, 2493 (1964).
[2] M. Balkanski and J. des Cloizeaux, J. Phys. Radium **21**, 825 (1960).
[3] J. A. Valdmanis, R. L. Fork, and J. P. Gordon, Opt. Lett. **10**, 131 (1985).
[4] C. Hirlimann, O. Seddiki, J.-F. Morhange, R. Monet, and A. Goddi, Opt. Commun. **59**, 52 (1986).
[5] C. Hirlimann, in *Femtosecond Laser Pulses*, edited by C. Rullière (Springer-Verlag, Berlin, 1998), p. 99.
[6] R. L. Fork, C. V. Shank, C. Hirlimann, R. Yen, and J. Tomlinson, Opt. Lett. **8**, 1 (1983).
[7] E. Gutsche and J. Voigt, in *Proceedings of the 7th International Conference on II-VI Semiconducting Compounds, Providence, R. I.*, edited by D. G. Thomas (W. A. Benjamin Inc., New York, 1967), p. 337.
[8] V. V. Sobolev, V. I. Donetskina, and E. F. Zagainov, Fiz. Tekh. Poluprovodn. **12**, 1089 (1978) [Sov. Phys. Semicond. **12**, 646 (1978)].
[9] F. Urbach, Phys. Rev. **92**, 1324 (1953).
[10] J. Dow, in *Optical Properties of Highly Transparent Solids*, Optical Physics and Engineering Series, edited by S. S. Mitra and B. Bendow (Plenum Press, New York, 1975), p. 131.
[11] O. Zakharov, A. Rubio, X. Blase, M. L. Cohen, and S. G. Louie, Phys. Rev. B **50**, 10 780 (1994), and references herein.
[12] J.J. Hopfield and D. G. Thomas, Phys. Rev. **122**, 35 (1961).
[13] D. G. Thomas, J. J. Hopfield, and M. Power, Phys. Rev. **119**, 570 (1960).
[14] D. G. Thomas and J. J. Hopfield, Phys. Rev. **128**, 2135 (1962).
[15] W. Kaiser and C. G. B. Garret, Phys. Rev. Lett. **7**, 229 (1961).
[16] V. Nathan, A. H. Guenther, and S. S. Mitra, J. Opt. Soc. Am. B **2**, 294 (1985).
[17] E. W. van Stryland, M. A. Woodall, H. Vanherzeele, and M. J. Soileau, Opt. Lett. **10**, 490 (1985).
[18] A. A. Said, M. Sheik-Bahae, D. J. Hagan, T. H. Wei, J. Wang, J. Wang, J. Young, and E. W. van Stryland, J. Opt. Soc. Am. B **9**, 405 (1992).
[19] C. Hirlimann, E. Wassmuth, E. Kling, S. Petit, and M. Pereira dos Santos, Appl. Phys. Lett. **65**, 959 (1994).
[20] M. Sheik-Bahae, D. C. Hutchings, D. J. Hagan, and E. W. van Stryland, IEEE J. Quantum Electron. **27**, 1296 (1991).
[21] B. Gross and J. T. Manassah, Opt. Commun. **126**, 269 (1996).
[22] J.-F. Lami, S. Petit, and C. Hirlimann, Phys. Rev. Lett. **82**, 1032 (1999).
[23] J.-F. Lami, P. Gilliot, and C. Hirlimann, Phys. Rev. Lett. **77**, 1632 (1996).
[24] A. E. Siegman, in *Lasers* (University Science Book, Mill Valley, California, 1986), p. 207.
[25] M. Cardona and G. Harbeke, Phys. Rev. **137**, A1467 (1965).
[26] A. I. A. Dahr and P. M. Lee, Phys. Scr. **38**, 441 (1988).
[27] X. Aymerich-Humet, F. Serra-Mestres, and J. Millan, Solid-State Electron. **24**, 981 (1981).
[28] Ch. Spiegelberg, J. Puls, and F. Henneberger, Phys. Status Solidi B **159**, 353 (1990).
[29] W. Rudolph, J. Puls, F. Henneberger, and D. Lap, Phys. Status Solidi B **159**, 49 (1990).
[30] G. R. Olbright, B. D. Fluegel, S. W. Koch, and N. Peyghambarian, in *Ultrashort Light Pulses: Picosecond Techniques and Applications*, Topics in Applied Physics Series Vol. 18, edited by S. L. Shapiro (Springer-Verlag, Berlin, 1977), p. 270.
[31] H.-E. Swoboda, F. A. Majumder, V. G. Lyssenko, C. Klingshirn, and L. Banyai, Z. Phys. B **70**, 341 (1988).
[32] A. Penzkofer and W. Falkenstein, Opt. Commun. **16**, 247 (1976).
[33] C. Hirlimann, J. F. Morhange, M. A. Kanahisa, A. Chevy, and C. H. Brito Cruz, Appl. Phys. Lett. **55**, 2307 (1989).
[34] H.-E. Swoboda, M. Sence, F. A. Majumder, M. Rinker, J.-Y. Bigot, J. B. Grun, and C. Klingshirn, Phys. Rev. B **39**, 11 019 (1989).
[35] J. Shah, Solid-State Electron. **21**, 43 (1978).
[36] M. C. Downer and C. V. Shank, Phys. Rev. Lett. **56**, 761 (1986).
[37] E. C. Fox and H. M. van Driel, in *Ultrashort Processes in Condensed Matter*, edited by W. E. Bron (Plenum Press, New York, 1993), Vol. B314, pp. 1, 22.
[38] S. M. Oak, K. S. Brinda, R. Chari, and C. Rustagi, J. Opt. Soc. Am. B **10**, 613 (1993).
[39] G. P. Banfi, V. Degiorgio, M. Ghigliazza, H. M. Tan, and A. Tomaselli, Phys. Rev. B **50**, 5699 (1994).
[40] E. C. Fox, E. J. Canto Said, and H. M. van Driel, Appl. Phys. Lett. **59**, 1878 (1991).
[41] J. H. Wilkinson and C. Reinsch, in *Linear Algebra*, edited by F. L. Bauer, Handbook for Automatic Computation Vol. II (Springer-Verlag, Berlin, 1971), p. 303.
[42] H. Schwalb, C. Dörnfeld, E. O. Göbel, J. M. Hvam, C. Klingshirn, J. Kuhl, V. G. Lyssenko, F. A. Majumder, G. Noil, J. Nunnenkamp, K. H. Pantke, R. Renner, A. Reznitsky, U. Siegner, H. E. Swoboda, and Ch. Weber, Phys. Status Solidi B **172**, 479 (1992).
[43] J. A. Kash, J. C. Tsang, and J. M. Hvam, Phys. Rev. Lett. **54**, 2151 (1985).
[44] D. von der Linde and R. Lambrich, Phys. Rev. Lett. **42**, 1090 (1979).
[45] V. S. Dneprovskii, V. I. Klimov, and M. G. Novikov, Zh. Eksp. Teor. Fiz. **99**, 843 (1991) [Sov. Phys. JETP **72**, 468 (1991)].
[46] I. M. Catalano, A. Cingolani, and A. Minafra, Phys. Rev. B **9**, 707 (1974).
[47] S. Petit, O. Crégut, and C. Hirlimann, Opt. Commun. **124**, 49 (1996).